JOURNAL OF GEOPHYSICAL RESEARCH, VOL. 102, NO. B3, PAGES 4957-4967, MARCH 10, 1997

Geodetic measurements of horizontal strain near the White Wolf fault, Kern County, California, 1926-1993

Gerald W. Bawden,[1] Andrea Donnellan,[2] Louise H. Kellogg,[1] Danan Dong,[2] and John B. Rundle[3]

Abstract. The White Wolf fault, located north of the Big Bend segment of the San Andreas fault, is the NE-SW trending, left lateral-oblique reverse fault responsible for the M_S=7.8 1952 Kern County earthquake. We combined Global Positioning System (GPS) measurements with historical triangulation and trilateration data to determine changes in the strain rate over 7 decades (1926-1993). We reanalyzed the historical geodetic data and calculated an elevated preseismic (1926-1952) maximum shear strain rate ($\dot{\gamma}$) of 0.62 ± 0.16 μstrain/yr across the White Wolf fault. The maximum shear strain rate decreased with distance toward the Garlock fault to 0.09 ± 0.08 μstrain/yr. In the decade following the earthquake (1952-1963), the near fault $\dot{\gamma}$ was high (0.85 ±0.23 μstrain/yr), and decreased to 0.23±0.13 μstrain/yr across the Garlock fault. In 1993, we resurveyed many of the same monuments with GPS receivers to estimate fault-crossing and off-fault strain rates for the preceding 30 years. Across the White Wolf fault, the maximum shear strain rate ($\dot{\gamma}$) dropped to 0.19±0.07 μstrain/yr. The azimuths of the maximum principal strain rates (ϕ) for the 1963-1993 epoch rotate from a fault normal orientation (-57° ±15°) across the White Wolf fault to 11° ±3°E across the Garlock fault.

Introduction

Since earthquakes occur relatively infrequently and the rates of strain across active seismogenic faults are usually small, the cyclic nature of earthquakes is poorly understood [*Sibson*, 1989]. To further understand the earthquake cycle and variations in the strain rate between earthquakes, we combined historic trilateration and triangulation data with Global Positioning System (GPS) observations to measure the interseismic deformation associated with the 1952 Kern County Earthquake (M_S=7.8) on the White Wolf fault in California (Figure 1) [*Gutenberg*, 1955; *Castillo and Zoback*, 1995]. Our combined data set spans 7 decades, allowing us to document the spatial and temporal distribution of changes in the shear strain rates throughout the White Wolf-Garlock fault region (Figure 2).

This paper presents the results of our GPS observations and analysis of GPS and historical data for the White Wolf network. We review the tectonic setting of the White Wolf fault and the seismicity of the region. For the geodetic analysis we used historical triangulation and trilateration data sets and GPS data collected in 1993. We present both the spatial and temporal distribution of the estimated strain rates for the network for the 2 and a half decades before the earthquake, the decade following the earthquake, and the most recent 3 decades. The results indicate that the strain rate is highest near the White Wolf fault, and that the strain rate varies with time near the fault (over the rupture plane). Rates were the highest during the decade following the earthquake.

[1]Department of Geology, University of California, Davis.
[2]Jet Propulsion Laboratory-California Institute of Technology, Pasadena.
[3]Cooperative Institute for Research in Environmental Sciences, University of Colorado, Boulder.

Paper number 96JB03554.
0148-0227/97/96JB-03554$09.00

Tectonic Setting

The White Wolf fault is located in the southern San Joaquin Basin, which is between the Sierra Nevada Mountains and the extensional Basin and Range Province to the east, and the transpressive California Coast Ranges and the Pacific-North America plate boundary to the west. Since the Pliocene epoch, there has been a transition in the southern San Joaquin Basin from an extensional to a contractional setting in response to the northward migration of the Mendocino Triple Junction and the formation of the San Andreas fault system [e.g., *Goodman*, 1989]. The White Wolf and Garlock faults are left-lateral faults that are conjugate to the Big Bend segment of the San Andreas fault. The oblique thrusting White Wolf fault results from regional compression and uplift of the Big Bend [*Stein and Thatcher*, 1981; *Eberhart-Phillips et al.*, 1990; *Snay et al.*, 1996].

The White Wolf fault partitions the southern San Joaquin Basin into two subbasins: the Maricopa subbasin and the Tejon embayment (Figure 1), with over 14 km of vertical structural relief between the Maricopa subbasin and the Tehachapi Mountains [*Goodman and Malin*, 1992]. Current regional contraction is evident in the Tejon embayment, which is ringed with several compressional structures and faults (Figure 1): the White Wolf fault to the north, the Comanchi Point thrust to the east, the Pleito thrust system along the south, and the Wheeler Ridge thrust to the southwest. Both Wheeler Ridge and Comanchi Point are active thrust-fault-cored anticlines [*Medwedeff*, 1988; *Goodman*, 1989].

Seismicity

The 1952 M_S=7.8 Kern County earthquake was the largest event in California following the 1906 ~M_S =8.3 San Francisco earthquake [*Castillo and Zoback*, 1995]. The 1952 event nucleated 18-20 km below Wheeler Ridge and propagated northeast along a 60 km section of the White Wolf

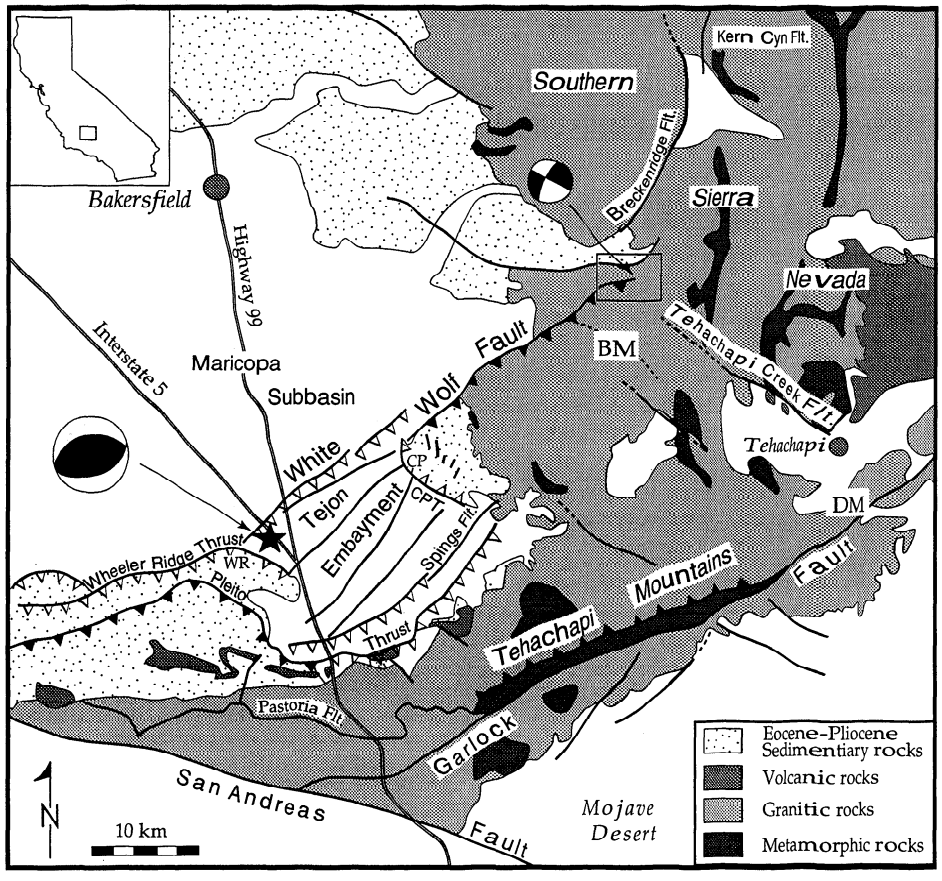

Figure 1. Basement complex and fault map of the southern San Joaquin Valley. Barbs represent exposed thrusts (closed) and blind thrusts (open). Star indicates the 1952 epicenter; focal mechanism is after *Wallace and Junkyoung* [1989]. Focal mechanism near the center of the figure is for M2 and M3 earthquakes for the region in the box [after *Castillo and Zoback,* 1995]. Abbreviations are CPT, Comanchi Point thrust; BM, Bear Mountain; DM, Double Mountain; and Flt, Fault. Modified from *Smith* [1964], *Jennings and Strand* [1969], and *Goodman and Malin* [1992].

fault (Figure 1) [*Gutenberg*, 1955; *Webb and Kanamori*, 1985; *Castillo and Zoback*, 1995]. The complex surface rupture and aftershock sequence showed both reverse and left-lateral offset on a southeast dipping fault [*Dibblee*, 1955; *Buwalda and St. Armand*, 1955]. Geodetic surveys found that the Bear Mountain (Figure 1) region rose about 1 m relative to the San Joaquin Valley and translated about 0.5 m toward the north-northeast relative to Double Mountain [*Whitten*, 1955; *Stein and Thatcher*, 1981]. A dislocation model of *Dunbar et al.* [1980] indicates that the mainshock caused 2.4 m of left-lateral slip and 1.9 m of reverse dip slip.

The southern San Joaquin Valley has remained seismically active since the Kern County earthquake in 1952, particularly near the epicentral region of the mainshock and the north-eastern end of the surface rupture [*Castillo*, 1993]. The microseismicity in the epicentral region tends to be infrequent; the earthquakes are generally larger than M 3.0 and nucleate as deep as 25 km [*Castillo*, 1993; *Castillo and Zoback*, 1994]. In contrast, the microseismicity near the northeastern terminus tends to be more frequent than on the southwestern segment; the events are generally smaller than M 3.0 in magnitude and are almost never deeper than 12 km [*Castillo*, 1993]. *Castillo and Zoback* [1995] describe this microseismicity as "late aftershocks" to the 1952 event.

Historical and Modern Geodetic Data

We combined our GPS observations with historical geodetic data, dating back to 1926, to determine variations in the spatial and temporal strain rates throughout the White Wolf-Garlock fault region. The historical data included United States Coast and Geodetic Survey (USC&GS) triangulation and deflection-of-vertical data (1926-1974), trilateration (1963-1979), and historical United States Geological Survey (USGS) trilateration data (1975-1989). Table 1 summarizes the data; the USC&GS data for the Tehachapi region are described in detail by *Bawden* [1995], and the USGS data are described by *Savage et al.* [1987], *Lisowski et al.* [1991], and *Dong* [1993].

In 1993 we collected GPS data for 13 monuments in the 25-monument Tehachapi Trilateration Network used by *Dunbar et al.* [1980] and *Stein and Thatcher* [1981] to analyze the spatial distribution of strain after the Kern County earthquake (Figure 2). The monuments for the GPS occupation were chosen based on the quantity of historical data, the position within the network, existence and access to the monument, and the potential contamination of the tectonic signal from groundwater and hydrocarbon withdrawal. Monuments on the east side of the Garlock fault were not used in the *Dunbar et al.* [1980] and *Stein and Thatcher* [1981] analyses but have been

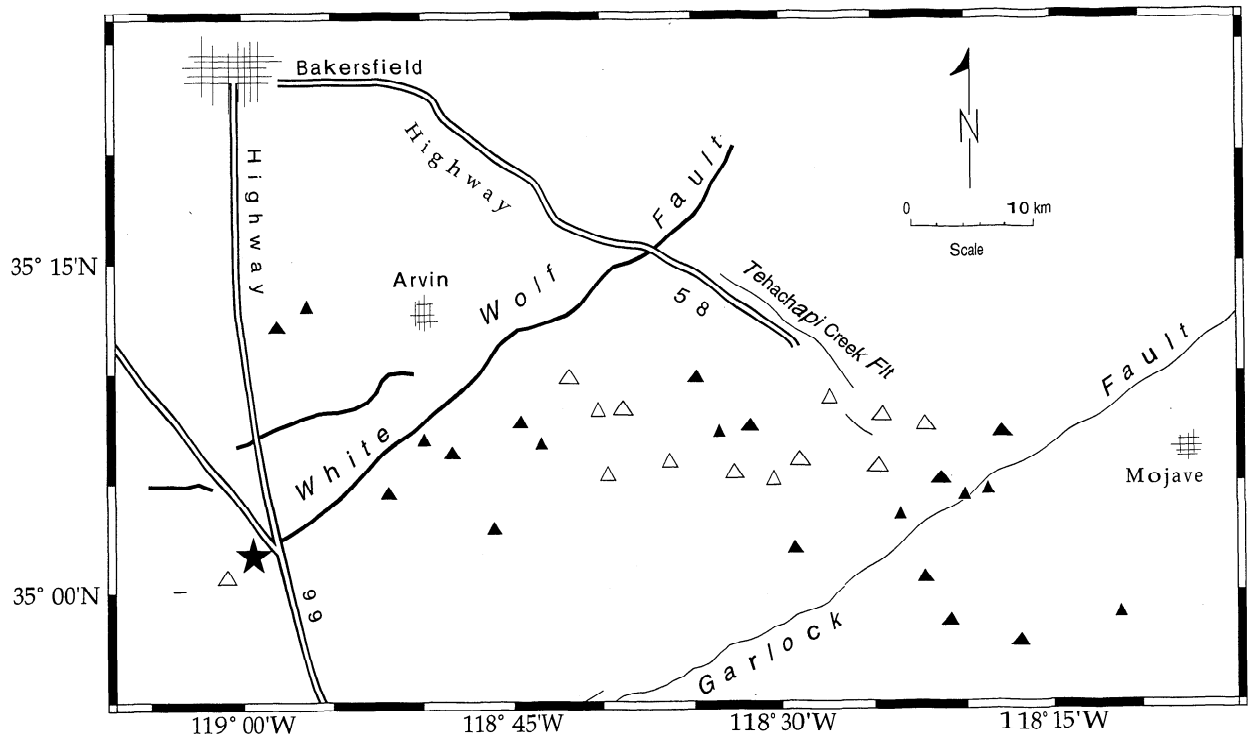

Figure 2. Monuments used in the strain analysis. Open triangles were occupied with GPS in 1993. All of the monuments have triangulation data. The heavy lines along the White Wolf fault are the surface ruptures from the 1952 Kern County earthquake, and the star indicates the epicenter for the mainshock [*Castillo and Zoback* , 1995].

analyzed by *Eberhart-Phillips et al.* [1990] and *King and Savage* [1984].

Data Analysis

The GPS data were processed with the software program GIPSY/OASIS II [*Webb and Zumberge*, 1993]. We fixed the satellite orbits using Jet Propulsion Laboratory (JPL) precise ephemerides and included continuously collected data from nearby well-determined GPS stations (JPL--Mesa (JPLM), Goldstone (GOLD), and Pinyon Flat Observatory (PIN1)) in our analysis of the GPS data collected during the field occupation. The average repeatabilities between subsequent station surveys were 3.2 mm for the east, 3.5 mm for the north, and 10.4 mm for the vertical components of the station's position.

Table 1. Geodetic Data Used in Each Epoch

Epoch	Stations	Observations	Outliers
Preseismic	triangulation		
1926, 1931-1932, 1938, 1940-1941, 1947-1952	84	1658	0
Immediate postseismic			
1952.75, 1953,1956, 1958-1960, 1963	84	1849	20
Most Recent			
1963, 1964, 1966-1967, 1971-1972, 1974	92	1013	10
	trilateration		
USC&GS 1962-1965, 1967, 1969-1977	32	293	38
	trilateration		
USGS 1975, 1980-1983, 1985, 1989	17	307	0
GPS	GPS	GPS days	0
July 1993	13	29	

"Stations" are the number of unique monuments used to calculate the strain rates for the given data type. For data sets that span several epochs, data were not necessarily collected for each monument in every epoch but were collected in at least 2 epochs. The USC&GS data for the Tehachapi region are described in detail by *Bawden* [1995], and the USGS data are described by *Savage et al.* [1987], *Lisowski et al.* [1991], and *Dong* [1993].

We used foward modeling network deformation analysis software [*Dong*, 1993] to estimate the strain rate parameters from the combination of historical triangulation, trilateration, and GPS data. The major differences between our method and *Dunbar et al.'s* [1980] method [*Frank*, 1966] are twofold: first, we combined multiple types of geodetic measurements to estimate deformation parameters. Second, we estimate site velocities of the whole network simultaneously, then derive the strain rate parameters for each subnetwork based on the site velocities, rather than calculate the strain rate parameters for each subnetwork separately. Thus the correlations of the estimated strain rate parameters between subnetworks are taken into account. Unlike GPS data, triangulation and trilateration data are unable to resolve the network rotation and translation rates. Triangulation data also have a rank deficiency for scale, therefore we set very loose constraints on positions and velocities at all triangulation and trilateration sites to avoid overconstraining and biasing our estimates of the strain rate parameters. Thus the velocities at these terrestrial survey sites are poorly determined, but the strain rate parameters are still well determined.

Triangulation measurements that exceeded 45 arcs (about 4.36 m for a 20 km baseline length observation) from the a priori position were removed as outliers. Table 1 shows the

number of observations that were removed in this manner. All of the trilateration data were converted from measured distances to baseline rates to reduce inherent errors caused by overconstraining a fixed system of monuments and to avoid possible biases between Geodolite and GPS data [*Savage et al.*, 1994]. The error model for the trilateration data was based on *Savage and Prescott* [1973] and has been used in several recent studies: *Johnson et al.* [1994], *Dong* [1993], and *Savage and Lisowski* [1995]. The GPS data were constrained by the formal errors from the GPS data analysis.

The results from our study were derived using the formulation of the extended Frank's method [*Frank*, 1966; *Prescott*, 1976; *Prescott et al.*, 1979; *Dong*, 1993]. The principal shear strain rates ($\dot{\gamma}_1$ and $\dot{\gamma}_2$), the maximum shear strain rate ($\dot{\gamma}$), and the azimuth of the maximum principal strain rate (ϕ) are

$$\dot{\gamma}_1 = \dot{E}_{ee} - \dot{E}_{nn} \tag{1}$$

$$\dot{\gamma}_2 = 2\dot{E}_{en} \tag{2}$$

$$\dot{\gamma} = \sqrt{\dot{\gamma}_1^2 + \dot{\gamma}_2^2} \tag{3}$$

$$\phi = \frac{1}{2}\tan^{-1}\left(\frac{\dot{\gamma}_2}{-\dot{\gamma}_1}\right). \tag{4}$$

where $\dot{E}_{nn}$ and $\dot{E}_{ee}$ are the diagonal components of the strain rate tensor in the north (n) and east (e) directions and $\dot{E}_{en}$ is the off-diagonal component. Positive $\dot{\gamma}_1$ values represent N-S pure shear with right-lateral shear across a vertical plane oriented at -45° or left-lateral shear across a vertical plane oriented at 45°. Positive $\dot{\gamma}_2$ values represent NW-SE pure shear with right-lateral shear across a vertical plane oriented at 90° or left-lateral shear across a vertical plane oriented at 0°. The maximum shear strain rate ($\dot{\gamma}$) is the highest shear rate, oriented 45° to the azimuth of the maximum principal strain rate ϕ [*Prescott et al.*, 1979]. All strain rates are given in units of microstrain per year (μstrain/yr), and ϕ is in units of degrees clockwise from north. All uncertainties are given as ±1 standard deviation.

Strain Rates for the Tehachapi Network

In the following section we describe the strain rates for 3 epochs: preseismic (1926-1952), immediate postseismic (1952-1963), and the most recent epoch (1963-1993). To determine how the strain rate parameters varied with distance from the White Wolf fault, we broke the network into four regional subnetworks, shown in Figure 3. These subnetworks were spaced at even distances from the White Wolf fault and each contained at least eight monuments. (Distances given are measured normal to the White Wolf fault.) We assume that all of the estimated strain rates are due to local deformation and not from regional strain that may be due to the nearby San Andreas fault. On the basis of a dislocation model using model parameters for the Big Bend segment of the San Andreas described by *Feigl et al.* [1993], we estimate that the San Andreas fault would contribute about 0.13 μstrain/yr at the southwestern end of the White Wolf fault.

Spatial Distribution of the Strain Rate Parameter Estimates for the Preseismic Epoch (1926-1952)

We evaluated the spatial distribution of the maximum shear strain rate ($\dot{\gamma}$) and the azimuth of maximum principal strain rate (ϕ) for the 26 year period preceding the Kern County earthquake. Only triangulation data were used for this epoch (Table 2). Figure 4a shows the spatial distribution of

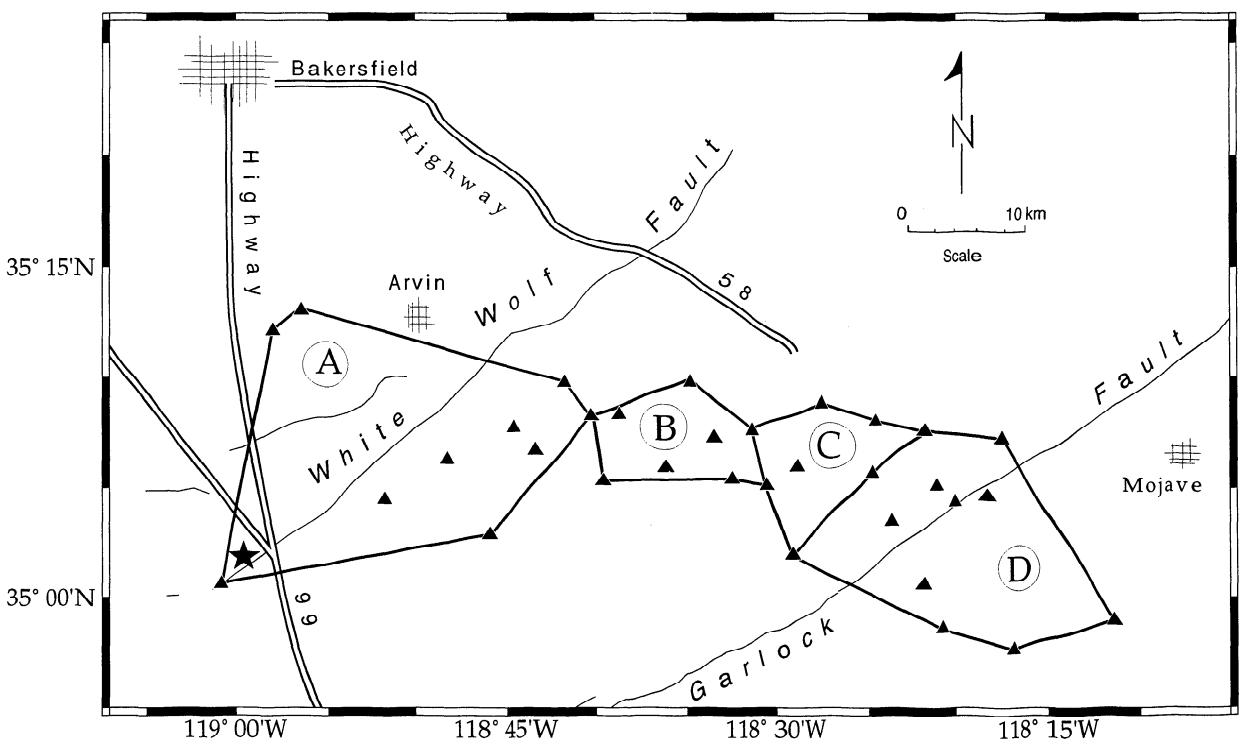

Figure 3. Monument combinations that define the regional networks. Strain and strain rate estimates were calculated from every monument with a minimum of two observations during the given epoch. Star indicates the 1952 epicenter.

Table 2. Strain Rate Estimates for the Preseismic, Coseismic, Immediate Postseismic and Most Recent Epochs

	Strain Rate Components, μstrain/yr					ϕ, degrees
Epoch/Region	$\dot{\varepsilon}_{ee}$	$\dot{\varepsilon}_{nn}$	$\dot{\gamma}_1$	$\dot{\gamma}_2$	$\dot{\gamma}$	clockwise from north
1926-1952						
A			0.62 ±0.16	0.04 ±0.15	0.62 ±0.16	-1 ±07
B			0.28 ±0.14	0.08 ±0.12	0.30 ±0.14	-8 ±10
C			-0.09 ±0.15	-0.03 ±0.15	0.10 ±0.15	82 ±40
D			0.07 ±0.08	-0.05 ±0.08	0.09 ±0.08	18 ±26
1952-1963						
A			-0.06 ±0.25	0.85 ±0.23	0.85 ±0.23	-47 ±08
B			0.51 ±0.22	0.00 ±0.19	0.51 ±0.22	0 ±11
C			0.13 ±0.21	0.14 ±0.19	0.20 ±0.20	-24 ±28
D			0.20 ±0.13	-0.10 ±0.14	0.23 ±0.13	13 ±18
1963-1993						
A	-0.04 ±0.05	-0.23 ±0.04	-0.09 ±0.12	0.17 ±0.05	0.19 ±0.07	-57 ±15
B			0.03 ±0.09	0.11 ±0.08	0.11 ±0.08	-36 ±20
C			0.27 ±0.05	-0.06 ±0.05	0.29 ±0.05	6 ±04
D	0.05 ±0.01	-0.05 ±0.02	0.10 ±0.03	-0.04 ±0.02	0.10 ±0.03	11 ±03

Here $\dot{\varepsilon}_{ee}$ is the maximum principal strain rate in the direction of ϕ (extension positive). $\dot{\varepsilon}_{nn}$ is the minimum principal strain rate, orthogonal to ϕ. Region A, B, C, D shown in Figure 3. All uncertainties are given as ±1 standard deviation.

maximum shear strain rate for the 1926-1952 epoch. Overall, maximum shear strain rates decrease with increased distance from the White Wolf fault. The maximum shear strain rate ($\dot{\gamma}$) in region A, near the White Wolf fault, is 6 times larger than the $\dot{\gamma}$ values for region D, near the Garlock fault. The orientations of ϕ for most of the subnetworks are approximately north-south (Figure 4b; Table 2).

Spatial Distribution of the Strain Rate Parameter Estimates for the Immediate Postseismic Epoch (1952-1963)

The spatial distribution of the maximum shear strain rate normal to the White Wolf fault (Figure 5a) for this epoch is similar to the preseismic (1926-1952) epoch, but elevated. As with the preseismic epoch, the subnetwork with the largest $\dot{\gamma}$ spanned the White Wolf fault, with $\dot{\gamma}$ values 3 to 4 times greater than in the network nearest the Garlock fault (Table 2). The maximum shear strain rates drop with distance from the White Wolf fault. The azimuths of the maximum principal strain rates for the immediate postseismic epoch rotate from a fault normal orientation (-47° ± 8°) across the White Wolf fault (region A) to an orientation that is east of north (13° ± 18°) across the Garlock fault (region D) (Figure 5b). We calculated an average $\dot{\gamma}$ for the monuments in regions A, B, and C of 0.51 ± 0.11 μstrain/yr, which is within the uncertainties of the value (0.80 ± 0.20 μstrain/yr) obtained by *Dunbar et al.* [1980] for the same epoch and similar monument combination.

Spatial Distribution of the Strain Rate Parameter Estimates for the Most Recent Epoch (1963-1993)

Overall, the regional maximum shear strain rates for this epoch have decreased since the 1952-1963 epoch, with an average maximum shear strain rate of 0.22 ± 0.04 μstrain/yr for the entire network. This network $\dot{\gamma}$ average is within the uncertainties of nearby rates from *King and Savage* [1984] ($\dot{\gamma}$=0.17± 0.02 μrad/yr, 1973-1983) and *Eberhart-Phillips et al.* [1990] ($\dot{\gamma}$=0.19± 0.01 μrad/yr, 1973-1987). Both of these studies evaluated trilateration data for a network of monuments that span the Garlock fault region east of the White Wolf fault and north of the San Andreas fault.

Figure 6a shows the spatial distribution of $\dot{\gamma}$ with distance from the White Wolf fault for the 1963-1993 epoch. We no longer observe a drop in the maximum shear strain rate as we move away from the White Wolf fault. Across the White Wolf, $\dot{\gamma}$, which was greatest during the 1952-1963 epoch, is now at its lowest value. In the Bear Valley region (region B, Figure 3), $\dot{\gamma}$ has also dropped significantly since the 1926-1952 and 1952-1963 epochs (Figure 6a). The maximum shear strain rates near the Garlock fault (regions C and D) remain unchanged from the previous epochs. The maximum shear strain rate for the Garlock region (region D, Figure 3) has returned to the pre-Kern County earthquake magnitudes.

The azimuth of maximum principal strain rate (ϕ) can be used to determine the orientation of contraction in a given region. This is only possible for the most recent epoch because trilateration and GPS data can determine the dilational component of strain. In a region with spatially uniform strain one would expect little change in ϕ. However, near the White Wolf fault, there are three major interacting faults: the San Andreas, Garlock, and White Wolf faults. Figure 6b shows the spatial distribution of ϕ for the 1963-1993 epoch. Overall, ϕ rotates 68°, from a fault normal orientation across the White Wolf fault to an east of north orientation across the Garlock fault. The ϕ orientations for regions A and B generally agree with P axis orientations calculated by *Castillo and Zoback* [1995] for the southern San Joaquin Valley and the White Wolf fault region. The geodetically determined ϕ orientation for the White Wolf fault region has a higher component of fault normal contraction than the range of

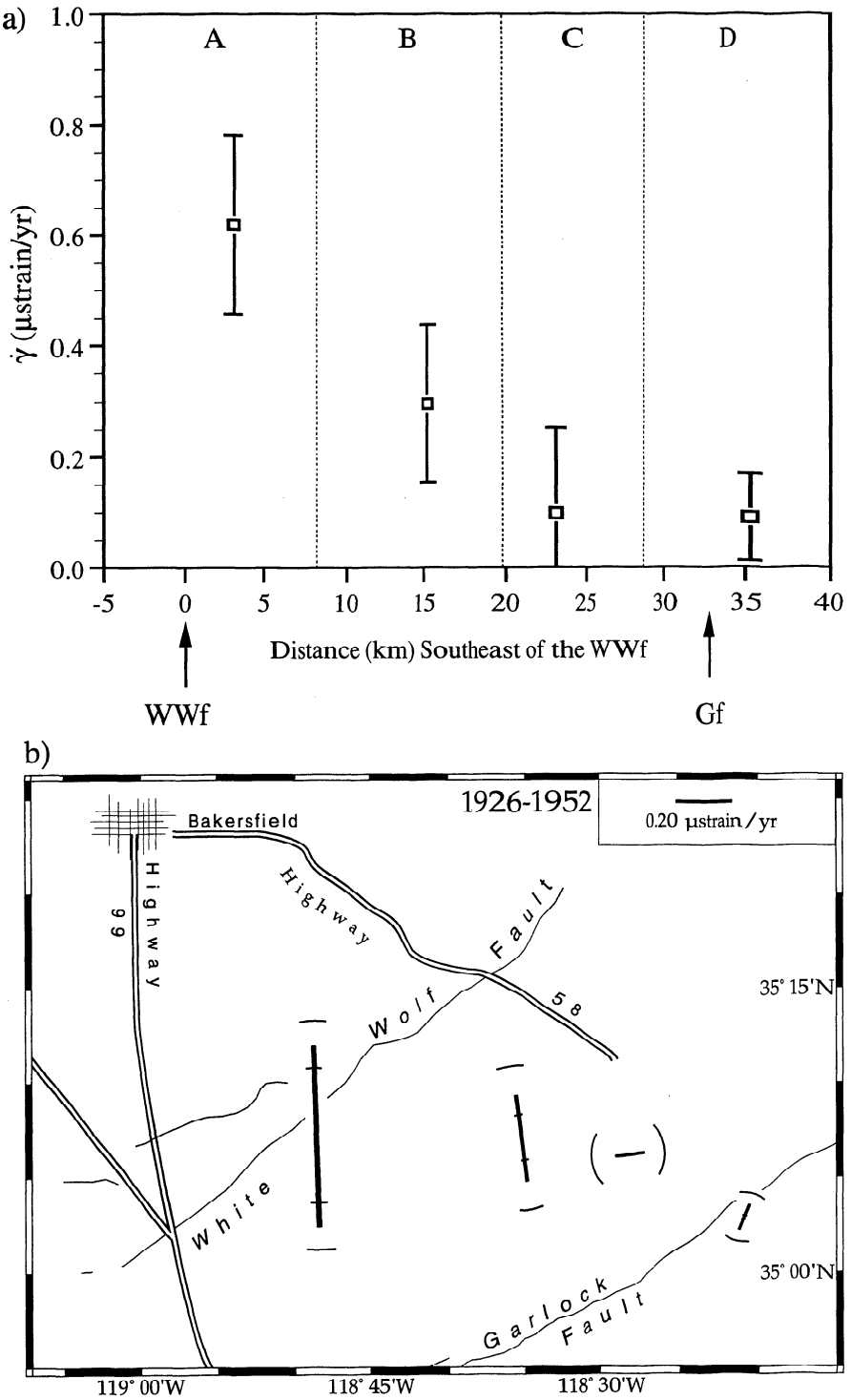

Figure 4. Spatial distribution of (a) the maximum shear strain rate ($\dot{\gamma}$) and (b) the azimuth of maximum principal strain rate (ϕ) scaled by maximum shear strain rate ($\dot{\gamma}$) for the 1926-1952 epoch. All distances are normal to the White Wolf fault with increasing distance to the southeast. Strain rates were calculated using all available monuments in each regional subnetworks. Vertical lines distinguish between adjacent regional subnetworks (Shown in Figure 3). All uncertainties are given as ±1 standard deviation. Arcs in Figure 4b are the 1σ angle and magnitude uncertainties. Abbreviations are WWf, White Wolf fault; Gf, Garlock fault.

seismically determined values. The ϕ values for the bear Valley Region agree, within the limit of the uncertainties, with the P axis orientation for the same region. The region between the White Wolf and Garlock faults has a ϕ orientation of north-south (0° ± 4°). This agrees well with values (-1.5° ± 2°) calculated by *Eberhart-Phillips et al.* [1990] for a similar region to the 1973-1987 epoch. The average orientation of ϕ for regions A, B, and C (-18° ± 3°), which spans west from the

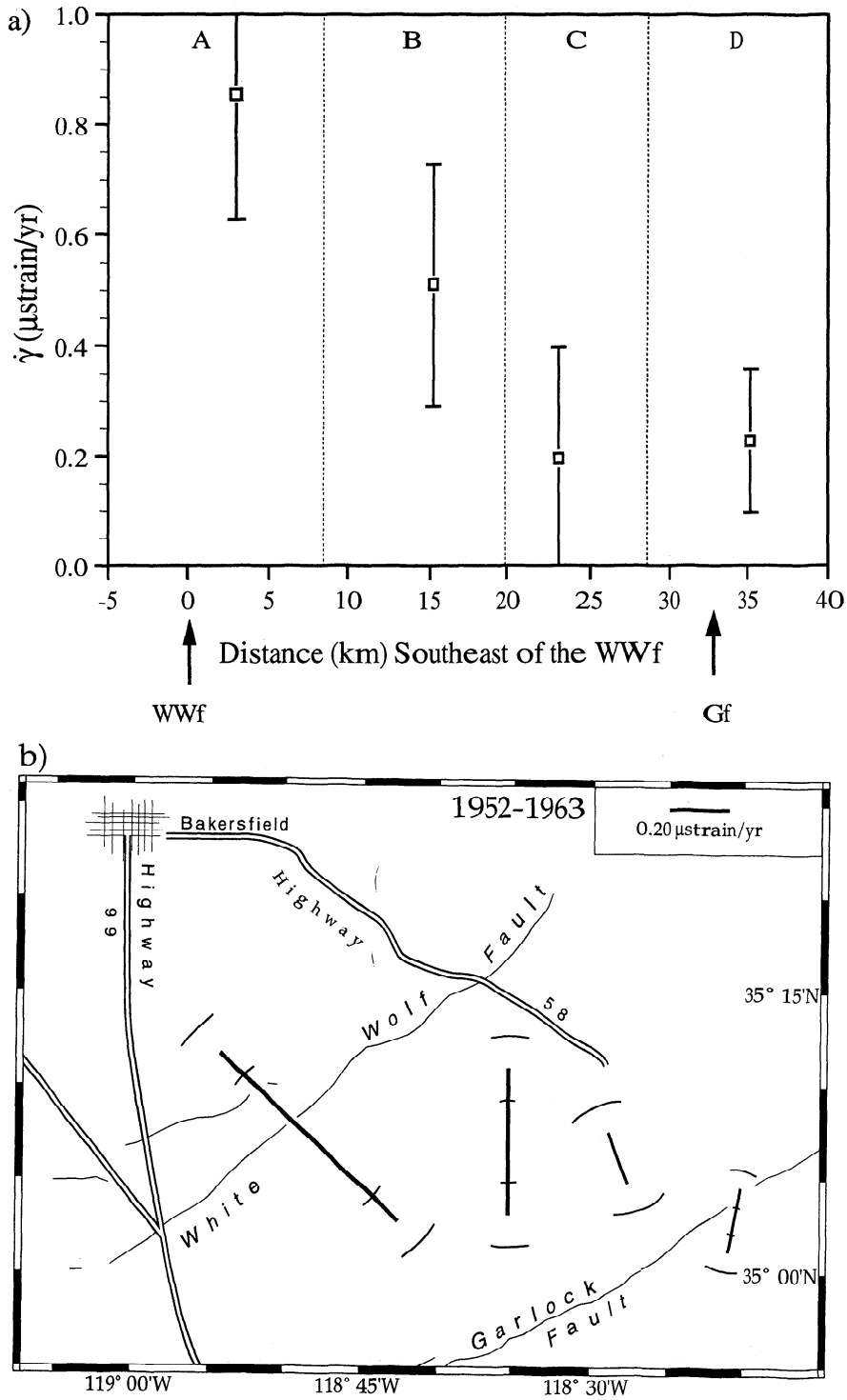

Figure 5. Spatial distribution of the (a) maximum shear strain rate and (b) azimuth of maximum principal strain rate for the 1952-1963 epoch. Notation is the same as Figure 4.

Garlock fault across the White Wolf fault, agrees well with -14° ± 4° calculated from *Prescott et al.* [1979] for the 1970-1978 epoch.

Strain Rate Through Time

Changes in the magnitude of the maximum shear strain rate over time disclose patterns within the regional subnetworks that we believe are related to the Kern County earthquake. Figure 7 shows variations in $\dot{\gamma}$ during 3 time intervals—1926-1952, 1952-1963, and 1963-1993 for the four regional subnetworks. Near the White Wolf fault there has been a significant drop in the maximum shear strain rate since the decade following the 1952 main shock. The maximum shear strain rate in region A was high for both the preseismic (1926-1952) and immediate postseismic (1952-1963) epochs, but dropped significantly for the 1963-1993 epoch. The maxi-

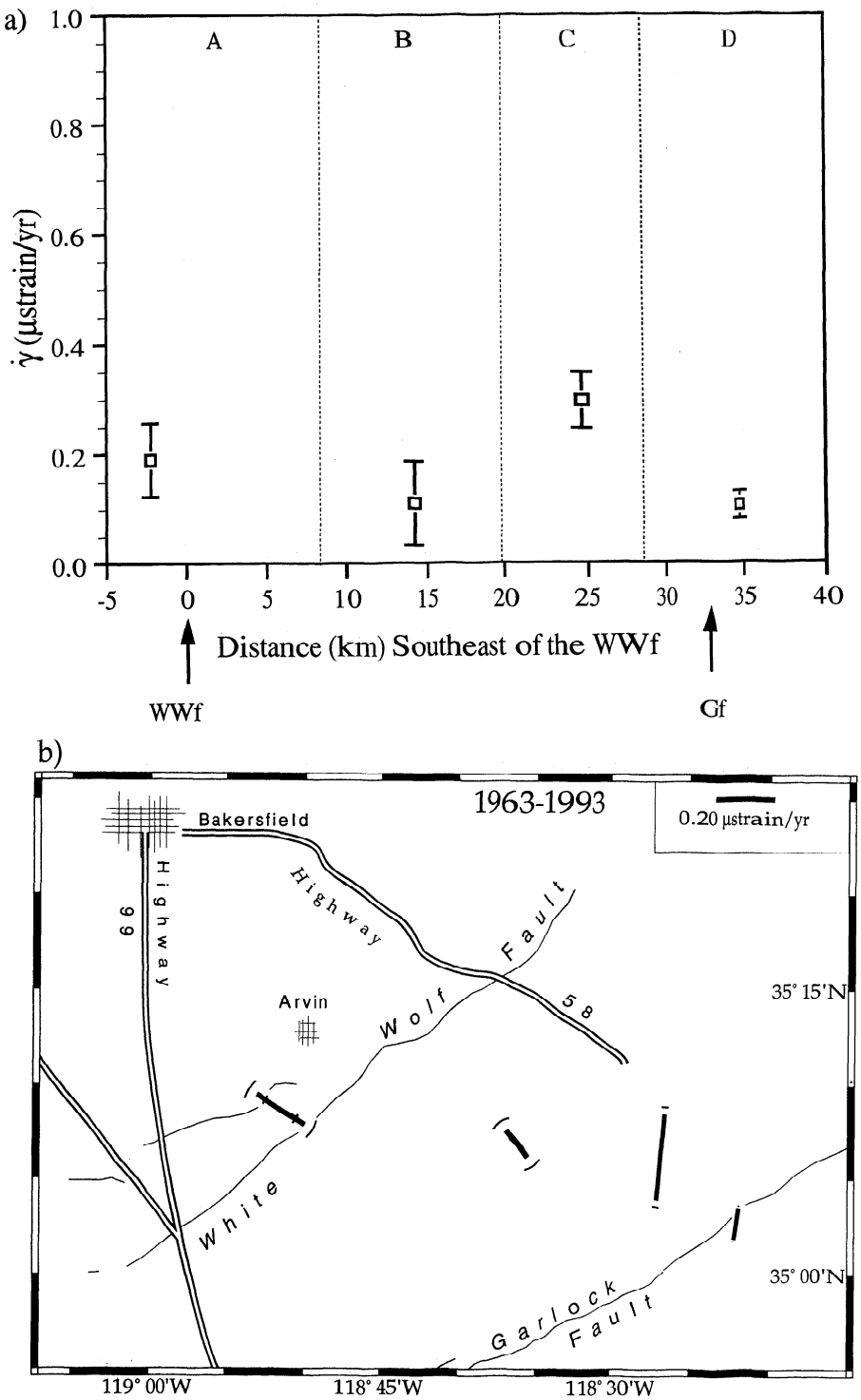

Figure 6. Spatial distribution of the (a) maximum shear strain rate and (b) azimuth of maximum principal strain rate for the 1963-1993 epoch. Notation is the same as Figure 4.

mum shear strain rates for region B, which had elevated strain rates for both the preseismic (1926-1952) and immediate postseismic (1952-1963) epochs, subsided during the 1963-1993 epoch. The maximum shear strain rates for regions C and D (near the Garlock fault) have changed little over the last 7 decades and are essentially the same now as they were during the 1926-1952 epoch.

Summary of Results

The maximum shear strain rates have varied both in space and time throughout the 7 decades of geodetic observations. For the preseismic epoch (1926-1952), strain rates near the White Wolf fault were higher than strain rates farther from the fault (Figure 4), and the azimuths of maximum principal strain

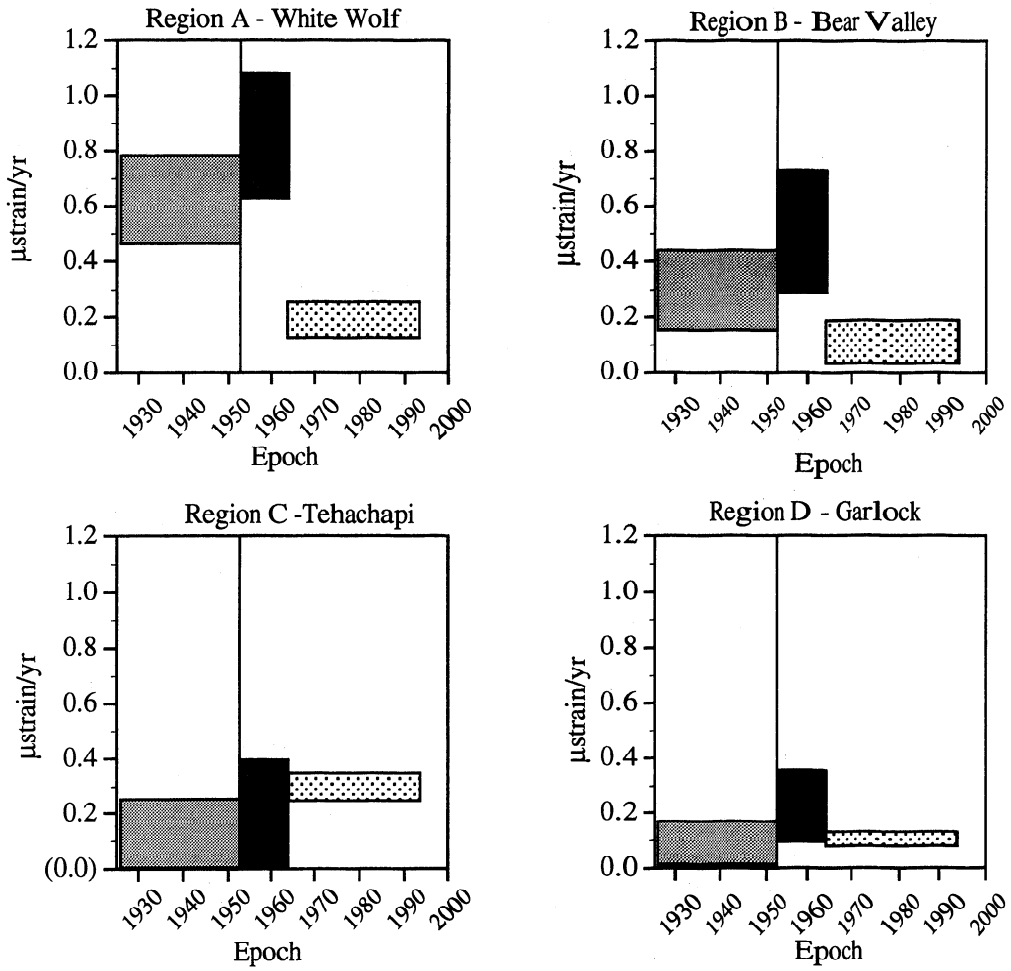

Figure 7. Variations in $\dot{\gamma}$ for 3 epochs (1926-1952, 1952-1963, and 1963-1993). Vertical height of boxes are 1σ errors for the strain calculations. Boxes span the time frame of the data set. The vertical line indicates the date of the Kern County earthquake (1952).

rate were predominately north-south. Strain rates during the 10 years following the earthquake (1952-1963) were similar to the preseismic strain rates, with the highest regional $\dot{\gamma}$ nearest the White Wolf fault. Strain rates during this epoch decrease with increasing distance southeast of the White Wolf fault. The average azimuth of maximum principal strain rate rotated slightly to west of north. During the 1963-1993 epoch the $\dot{\gamma}$ dropped for the two subnetworks near the White Wolf fault (Figure 3, regions A and B) and remained unchanged for the two southeastern subnetworks. The highest $\dot{\gamma}$ for this epoch was in the Tehachapi region (Figure 3, region C). The azimuth of maximum principal strain rate rotated progressively 68° from the subnetwork (A) that spans the White Wolf fault to the subnetwork (D) that spans the Garlock fault (Figure 6, Table 2).

Discussion

The highest observed strain rates occurred in the decade following the 1952 Kern County earthquake across the White Wolf fault ($\dot{\gamma}$=0.85±0.23 μstrain/yr). Presumably, this elevated maximum shear strain rate was caused by readjustment of the crust to the deformation associated with the mainshock. During the next 3 decades the measured strain rate across the White Wolf fault dropped significantly (0.19±0.07 μstrain/yr). The observed strain rates near the fault were also high during the 26 year period preceding the earthquake ($\dot{\gamma}$=0.62 ±0.16 μstrain/yr).

The most robust conclusion is that the strain rates were highest in the decade following the Kern County event. Most, but not all, of the response to the earthquake took place during the first decade after the quake. The strain rates that we observe during this time may be directly associated with afterslip on the fault or an extension of the fault plane. This conclusion is consistent with models of data collected for other earthquakes (e.g. Northridge, *A. Donnellan et al.*, in preparation; Loma Prieta, *Bürgmann et al.* [1996]). The orientation of maximum compression oriented perpendicular to the fault is consistent with updip slip occurring on the fault.

The strain rates observed prior to the earthquake are higher than those we observe at present. It is possible that the strain rate pattern is due to subsidence of the San Joaquin Valley from water withdrawal over this time period. Subsidence of the valley would cause east-west extension of the mountains to the east, consistent with the calculated strain orientation. Preliminary models of subsidence in the valley produce strain rates of a similar pattern and magnitude to those observed.

If the high strain rate near the fault prior to the earthquake is

actually associated with the earthquake cycle, some as yet unidentified process such as stress softening may cause increased deformation prior to the earthquake. Future observations and models will clarify whether accelerated deformation occurs prior to an earthquake. It is also possible that the calculated strain rates in the most recent epoch are, for some reason, lower than the actual strain rates. For example, the strain regime may have changed over the 30 years (e.g., rotation of compression axis) such that the calculated strain rates are lower than the actual strain rates from either early or late in the epoch. In the last epoch most of the strain we observed may be regional strain due to deep slip on the San Andreas fault. The region may no longer be responding the the White Wolf fault or to the 1952 earthquake. Future GPS observations will clarify the current style of deformation and provide better constraints on models of the earthquake cycle.

Acknowledgments. Funding was provided by a grant from the IGPP of Lawrence Livermore National Lab, a Presidential Faculty Fellowship from NSF, and a U. C. Davis Durrell Research grant. A portion of this research was carried out at the Jet Propulsion Lab, California Institute of Technology, with funding from NASA, the USGS and the Southern California Earthquake Center. We thank Roland Bürgmann, Eldridge Moores, Jim McClain, and Greg Lyzenga for helpful discussions, and Nancy King, Robert King, and an anonymous reviewer for constructive criticism and valuable suggestions that greatly improved the manuscript. We also wish to thank Ruth Neilan (JPL) for securing GPS receivers from both JPL and UNAVCO. GIPSY/OASIS II GPS data analysis software and training were provided by Ken Hurst at JPL. Michael Cline (SCEC), Richard Snay (NGS), and Duncan Agnew (UC San Diego) provided monument site information and the historical geodetic data. The services of Mark Smith and Garth Franklin, both at JPL, were invaluable for the field operations and training. We would also like to thank Paul Waterstraat, Kate Hill and Doug Neuhauser for their computer expertise. We are indebted to the following people for graciously allowing access to their property: John Yeakley, Jim Fontecchi, Jeff Stevenson, Dan Baer (C.E.O. of IBT International Inc.), Lars Oberg, Bud Armstead, Paul Blair, David Eckert, the Arbura's, Jim Mann, the Braley's, and Gary Onyshko. We wish to thank the following people for graciously helping in the GPS campaigns: C. Bawden, D. Dorritie, D. DiPietro, R. Garcia, C. Helm, D. Hunt, G. Lyzenga, B. Matthews, N. Montague, B. Rowen, G. VonDamm, and C. Williams.

References

Bawden, G. W., Geodetic measurements of four decades of horizontal strain near the White Wolf fault, Southern California, M.S. thesis, Univ. of California, Davis, 1995.

Bürgmann, R., P. Segall, M. Lisowski, and J. Svarc, Postseismic strain following the 1989 Loma Prieta Earthquake from GPS and leveling measurements, *J. Geophys. Res.*, in press, 1996.

Buwalda, J. P., and P. St. Armand, Geologic effects of the Arvin-Tehachapi earthquake, in *Earthquakes in Kern County California During 1952, Bulletin 171*, edited by G. Oakeshott, pp. 67-74, Calif. Div. of Mines, San Francisco, Calif., 1955.

Castillo, D., State of stress near active plate boundaries: The San Andreas fault in northern and central California, and the Indo-Australian plate, South of Java, Ph. D. thesis, Stanford Univ., Stanford, Calif., 1993.

Castillo, D., and M. D. Zoback, Systematic variations in stress state in the southern San Joaquin Valley: Inferences based on well-bore data and contemporary seismicity, *AAPG Bull., 78*, 1257-1275, 1994.

Castillo, D., and M. D. Zoback, Systematic stress variations in the southern San Joaquin Valley and along the White Wolf fault: Implications for the rupture mechanics of the 1952 M_S 7.8 Kern County earthquake and contemporary seismicity, *J. Geophys. Res.*, *100*(B4), 6249-6264, 1995.

Dibblee, T. W., Geology of the southeastern margin of the San Joaquin Valley, California, in *Earthquakes in Kern County California During 1952, Bulletin 171*, edited by G. Oakeshott, pp. 23-34, Calif. Div. of Mines, San Francisco, Calif., 1955.

Dong, D., The horizontal velocity field in southern California from a combination of terrestrial and space-geodetic data, Ph. D. thesis, Mass. Inst. of Technol., Cambridge, 1993.

Dunbar, W. S., D. Boore, and W. Thatcher, Pre-, co-, and postseismic strain changes associated with the 1952 M_L = 7.2 Kern County, California, Earthquake, *Bull. Seismol. Soc. Am., 70(5)*, 1893-1905, 1980.

Eberhart-Phillips, D., M. Lisowski, and M. Zoback, Crustal strain near the Big Bend of the San Andreas fault: Analysis of the Los Padres-Tehachapi trilateration networks, California, *J. Geophys. Res.*, *95*(B2), 1139-1153, 1990.

Feigl, K.L., et al., Space geodetic measurement of crustal deformation in central and southern California, 1984-1992, *J. Geophys. Res., B, 98*(B12), 21,677-21,712, 1993.

Frank, F. C., Deduction of earth strains from survey data, *Bull. Seismolo. Soc. Am., 56*, 35-42, 1966.

Goodman, E. D., The tectonics of transition along an evolving plate margin--Cenozoic evolution of the southern San Joaquin Basin, California, Ph.D. thesis, Univ. of Calif., Santa Barbara, 1989.

Goodman, E. D., and P. Malin, Evolution of the southern San Joaquin Basin and mid-Tertiary transitional tectonics, central California, *Tectonics, 11*(3), 478-498, 1992.

Gutenberg, B., The first motion on longitudinal and transverse waves of the main shock and the direction of slip, in *Earthquakes in Kern County California During 1952, Bulletin 171*, edited by G. Oakeshott, pp. 165-170, Calif. Div. of Mines, San Francisco, Calif., 1955.

Jennings, C., and R. Strand, Geologic map of California, Los Angeles Sheet, pp. 1:250,000, State of California, Dep. of Conserv., 1969.

Johnson, H.O., D.C. Agnew, and F.K. Wyatt, Present-day crustal deformation in southern California, *J. Geophys. Res.*, *99*(B12), 23,951-23,974, 1994.

King, N. E., and J. C. Savage, Regional deformation near Palmdale, California, 1973-1983, *J. Geophys. Res.*, *89*(B4), 2471-2477, 1984.

Lisowski, M., J.C. Savage, and W.H. Prescott, The velocity field along the San Andreas fault in central and southern California, *J. Geophys. Res.*, *96*(B5), 8369-8389, 1991.

Medwedeff, D. A., Structrual analysis and tectonic significance of late-Tertiary and Quaternary, compressive-growth folding, San Joaquin Valley, California, Dissertation thesis, Princeton Univ., Princeton, N. J., 1988.

Prescott, W. H., An extension of Frank's method for obtaining crustal shear strains from survey data, *Bull. Seismol. Soc. Am., 66*, 1847-1853, 1976.

Prescott, W. H., J .C. Savage, and W. T. Kinoshita, Strain accumulation rates in the western United States between 1970 and 1978, *J. Geophys. Res., 84*(B10), 5423-5435, 1979.

Savage, J.C., M. Lisowski, W.K. Gross, N.E. King, and J.L. Svarc, Strain accumulation near Yucca Mountain, Nevada, 1983-1993, *J. Geophys. Res., 99*(B9), 18,103-18,107, 1994.

Savage, J.C., and M. Lisowski, Interseismic deformation along the San Andreas fault in southern California, *J. Geophys. Res., 100*(B7), 12,703-12,717, 1995.

Savage, J.C., and W.H. Prescott, Precision of geodolite distance measurements from determining fault movements, *J. Geophys. Res., 78*(26), 6001-6008, 1973.

Savage, J.C., W.H. Prescott, and M. Lisowski, Deformation along the San Andreas fault, 1982-1986 as indicated by frequent Geodolite measurements, *J. Geophys. Res., 92*(B6), 4785-4797, 1987.

Sibson, R. H., Earthquake faulting as a structural presses, *J. Struct. Geol., 11* (1/2), 1-14, 1989.

Smith, A. R., Geologic map of California, Bakersfield Sheet, pp. 1:250,000, State of California, Depart. of Conserv., 1964.

Snay, R.A., M.W. Cline, and C.R. Philipp, Crustal velocity field near the big bend of California's San Andreas fault, *J. Geophys. Res., 101*(B2), 3173-3185, 1996.

Stein, R., and W. Thatcher, Seismic, aseismic deformation associated with the 1952 Kern County, California earthquake and relationship to Quaternary history of the White Wolf fault, *J. Geophys. Res., 86*(B6), 4913-4928, 1981.

Wallace, T. C., and K. Junkyoung, Inversion of complex seismic sources, in the effects of structure and source complexity on Waveforms: Crustal structure of Tibet and the recovery of complex

seismic sources, *Rep. GL-TR-89-0259,* Geophys. Lab., Air Force Syst. Command, 1989.

Webb, T. H., and H. Kanamori, Earthquake focal mechanisms in the Eastern Transverse Ranges and San Emigdio Mountains, southern California and evidence for a regional decollement, Bull. Seismol. Soci. Am., *75*(3), 737-757, 1985.

Webb, F.H., and J.F. Zumberge, *Introduction to GIPSY/OASIS-II,* Jet Propulsion Laboratory, Pasadena, Calif., 1993.

Whitten, C. A., Measurements of earth movements in California, in *Earthquakes in Kern County, California During 1952, Bulletin 171,* edited by G. Oakeshott, pp. 75-80, Calif. Div. of Mines, San Francisco, Calif., 1955.

G. W. Bawden and L. H. Kellogg, Deptartment of Geology, University of California, Davis, CA 95616. (email: bawden@geology.ucdavis.edu; kellogg@ymir.ucdavis.edu)

D. Dong and A. Donnellan, Jet Propulsion Laboratory-California Institute of Technology, Pasadena, CA 91109-8099. (email: dong@freia.jpl.nasa.gov; andrea@cobra.jpl.nasa.gov)

J. B. Rundle, CIRES, University of Colorado, Boulder, CO 80309. (email: rundle@hopfield.colorado.edu)

(Received March 15, 1996; revised November 8, 1996;
accepted November 12, 1996.)